Acta Cryst. (1994). B50, 465–472

X-ray Rietveld Structure Determination of Ammonium Rochelle Salt at 120 (Paraelectric Phase) and 100 K (Ferroelectric Phase)

BY Z. BROŻEK, D. MUCHA AND K. STADNICKA

Faculty of Chemistry, Jagiellonian University, Ingardena 3, 30-060 *Kraków, Poland*

(*Received* 12 *October* 1993; *accepted* 13 *January* 1994)

Abstract

Crystal structure of $NaNH_4(+)$-$C_4H_4O_6.4H_2O$ in both the paraelectric (at 120 K) and ferroelectric (at 100 K) phases, near the first-order phase transition at 109 K, was determined from X-ray powder data using the Rietveld refinement method. The largest relative displacements (greater than 0.30 Å) of atoms in the ferroelectric phase, compared with the paraelectric phase, were found for one of the water molecules, the ammonium cations and one of the hydroxyl groups. The structural mechanism of the ferroelectric phase transition seems to rely on a cooperative process of the reorientation of the ammonium cations and water dipoles and the reorganization of the complex hydrogen-bonding network. For the monoclinic ferroelectric phase, the value and sign of the spontaneous polarization vector $\mathbf{P}_s$ (parallel to **b**) was found from a point-charge model as $+0.22\,(1) \times 10^{-6}$ C cm^{-2} at 100 K.

Introduction

Sodium ammonium tartrate tetrahydrate (NAT) crystals are well known since they were the first of any compound separated as left- and right-handed optical enantiomers (Lowry, 1964). They are isomorphous with Rochelle salt (RS), $NaKC_4H_4O_6.4H_2O$, the first ferroelectric material discovered (Jona & Shirane, 1962), hence their name ammonium Rochelle salt (ARS). Unlike RS they undergo an improper ferroelectric–ferroelastic phase transition at about 109 K. The crystals reveal interesting physical properties, both in the paraelectric ($P2_12_12$) and ferroelectric ($P12_11$) phases, as summarized previously (see Table 1; Brożek & Stadnicka, 1994). Many theoretical concepts concerning the mechanism for the first-order phase transition have already been published (Aizu, 1971, 1984, 1986*a*,*b*, 1990; Sawada & Takagi, 1972; Ishibashi & Takagi, 1975; Sannikov & Levanyuk, 1977). Until now, none have been confirmed by crystal structure studies in the vicinity of the phase transition. The crystal structure of NAT at room temperature has been previously determined (Beevers & Hughes, 1941; Shkuratova, Kiosse & Malinovskii, 1979; Kuroda & Mason, 1981), but studies of its absolute structure have only recently been made in the low-temperature region of the paraelectric phase (Brożek & Stadnicka, 1994). For the ferroelectric phase, only a preliminary structure investigation has been made. X-ray oscillation photographs of NAT single crystals below the phase transition at 109 K show split reflections (evidence of the two possible ferroelectric domains) and reflections of the type $h \pm \frac{1}{2}$, k, l, resulting most probably from a doubling of the parameter a (Sawada & Takagi, 1971). Incommensurate satellite reflections of the types $h + n\delta$, k, 0 and $h + \frac{1}{2} + n\delta$, k, 0 were also found later, below the phase transition for a single crystal of deuterated NAT, $NaND_4C_4H_2D_2O_6.4D_2O$, with neutron diffraction scans between reflections 110 and 210 (Iizumi & Gesi, 1978). Moreover, the X-ray intensity was measured in the $hk0$ reciprocal layer at intervals of $a^*/10$ and $b^*/10$ for a single crystal of $NaNH_4(2R,3R)$-$C_4H_4O_6.4H_2O$ at 90 K (Brożek & Stadnicka, 1994; Appendix 1). Split reflections (120, 240 *etc.*), superlattice reflections, $3\frac{1}{2},1,0$, $3\frac{1}{2},3,0$, $2\frac{1}{2},3,0$, $3\frac{1}{2},2,0$, $3\frac{1}{2},4,0$ and $2\frac{1}{2},4,0$, as well as satellites of the type $h \pm \delta$, k, 0 and $h + \frac{1}{2} \pm \delta$, k, 0 were revealed.

Systematic studies of the crystal structure of NAT in the ferroelectric phase would seem necessary to understand the structural mechanism of the first-order phase transition. Unfortunately, single-crystal studies of the structure are hampered by twinning in the ferroelectric phase. We thus used X-ray powder methods and the results are presented here.

Experimental

NAT crystals were obtained in two steps. Disodium (+)-tartrate dihydrate and diammonium (+)-tartrate were produced by reacting (+)-tartaric acid with sodium and ammonium carbonates, respectively [L-(+)-tartaric acid, c.p., Na_2CO_3, c.p., $(NH_4)_2CO_3$, p.a.; Polskie Odczynniki Chemiczne). NAT crystals were then grown from an aqueous solution of a stoichiometric mixture of these tartrates in an ammonia/air atmosphere. Crystals of good optical quality were ground, placed in a glass capillary and

examined using the Guinier X-ray diffraction technique (Cu $K\alpha$ radiation) *vs* temperature. Guinier photographs, produced in the temperature range 83–143 K with different cooling rates, clearly showed a symmetry change at *ca* 110 K (*i.e.* at the ferroelectric–ferroelastic phase transition) and no remarkable changes within the paraelectric phase. From the photograph for a heating rate of 2.8 K h^{-1}, two X-ray diffraction patterns were chosen for the structure analysis at approximately 100 and 120 K, on either side of the phase transition, and scanned using an optical photometer. After an appropriate data transformation, refinements of both structures were carried out using an XRS82 system on a 486 PC (Mucha & Łasocha, 1994). Details of the Rietveld refinements are presented in Table 1.*

The background was determined by the linear interpolation from points chosen in between peaks as well as additionally generated by a quadratic interpolation. The background was not refined in the further procedure. The peak shape function was determined from the 410 peak of the pattern at 120 K. It was numerically applied for other peaks of both diffraction patterns and adjusted by four parameters (refined for each pattern separately) within two linear functions of 2θ: the peak width and the peak asymmetry.

A starting model for the orthorhombic phase was taken from the single-crystal X-ray data for NAT at 120 K (Brożek & Stadnicka, 1994). The refinement procedure was the following:

(1) only the scale factor;
(2) the scale factor and profile parameters without the unit-cell parameters;
(3) the scale factor and the unit-cell parameters;
(4) the scale factor and profile parameters, including the unit-cell parameters;
(5) as in (4), but positional and isotropic thermal parameters were refined alternately.

As an initial model of the structure of the monoclinic phase at 100 K, two molecules, related in the orthorhombic phase by the twofold axis, were taken with coordinates according to the single-crystal data at 120 K and the unit-cell parameters were assumed to be $a = 12.113$, $b = 14.406$, $c = 6.202$ Å and $\beta = 90.5°$. The non-standard setting with the origin at $\frac{1}{4}00$ for the space group $P12_11$ was chosen, so that a comparison with the orthorhombic structure could readily be made. The succeeding steps of the structure refinement were:

(1) the scale factor;
(2) the scale factor and β angle;
(3) the scale factor, β angle and zero correction parameters only;
(4) the scale factor and the profile parameters, including the unit-cell parameters;
(5) the scale factor together with the positional and isotropic thermal parameters, alternately.

The observed and calculated spectra are presented for both structures in Fig. 1. The refined atomic coordinates and isotropic temperature factors are listed in Table 2. Structural differences between the paraelectric and ferroelectric phases are presented in Fig. 2 (*ORTEP*; Johnson, 1971). The atom numbering is kept similar to that of the single crystal data published earlier (Kuroda & Mason, 1981; Brożek & Stadnicka, 1994). Geometric calculations were performed using the *PARST* program (Nardelli, 1983).

Table 1. *Summary of the structure refinements for* $NaNH_4(2R,3R)$-$C_4H_4O_6.4H_2O$ *crystals*, $M_r = 261.16$, *in the paraelectric* (120 K) *and ferroelectric* (100 K) *phases*; Cu $K\alpha_1$ *radiation*, $\lambda = 1.54056$ Å

	120 K	100 K
Space group	$P2_12_12$	$P12_11$
a (Å)	12.0762 (4)	12.1252 (2)
b (Å)	14.3621 (6)	14.4144 (2)
c (Å)	6.1829 (2)	6.1989 (1)
V (Å^3)	1072.4 (1)	1083.22 (3)
β (°)	90	91.0392 (1)
Pattern 2θ range (°)	16.1–97.0	16.1–97.0
Step scan increment (°)	0.02	0.02
Standard peak [hkl, 2θ(°)] for peak shape function	410, 30.34	410, 30.34
Number of steps	3624	3624
Number of contributing reflections	621	1081
Absorption correction	None	None
Extinction correction	None	None
Preferred orientation	None detected	None detected
Number of geometric restrictions*	21	42
Number of structural parameters	64	127
Number of profile parameters	9	10
R_{wp}	0.211	0.187
R_f	0.161	0.150
R_I	0.221	0.195
R_{exp}	0.294	0.269
Maximum shift/error	0.7	0.9

* Active soft restrictions with e.s.d.'s in parentheses for bond lengths

C—C	1.52 (1)
C—O hydroxylic	1.420 (12)
C—O carboxylic	1.250 (12) Å;

for bond angles within the tartaric anion according to the appropriate hybridization of C atoms: 120 (20) for sp^2 and 109 (25)° for sp^3.

Discussion

Important interatomic distances, bond lengths, bond angles and torsion angles are presented in Table 3. Within the limits of error, there are no significant differences between the appropriate bond lengths of the tartaric anion at 120 K established with the powder and single-crystal methods, whereas slight

* A list of powder diffraction data has been deposited with the IUCr (Reference: AB0318). Copies may be obtained through The Managing Editor, International Union of Crystallography, 5 Abbey Square, Chester CH1 2HU, England.

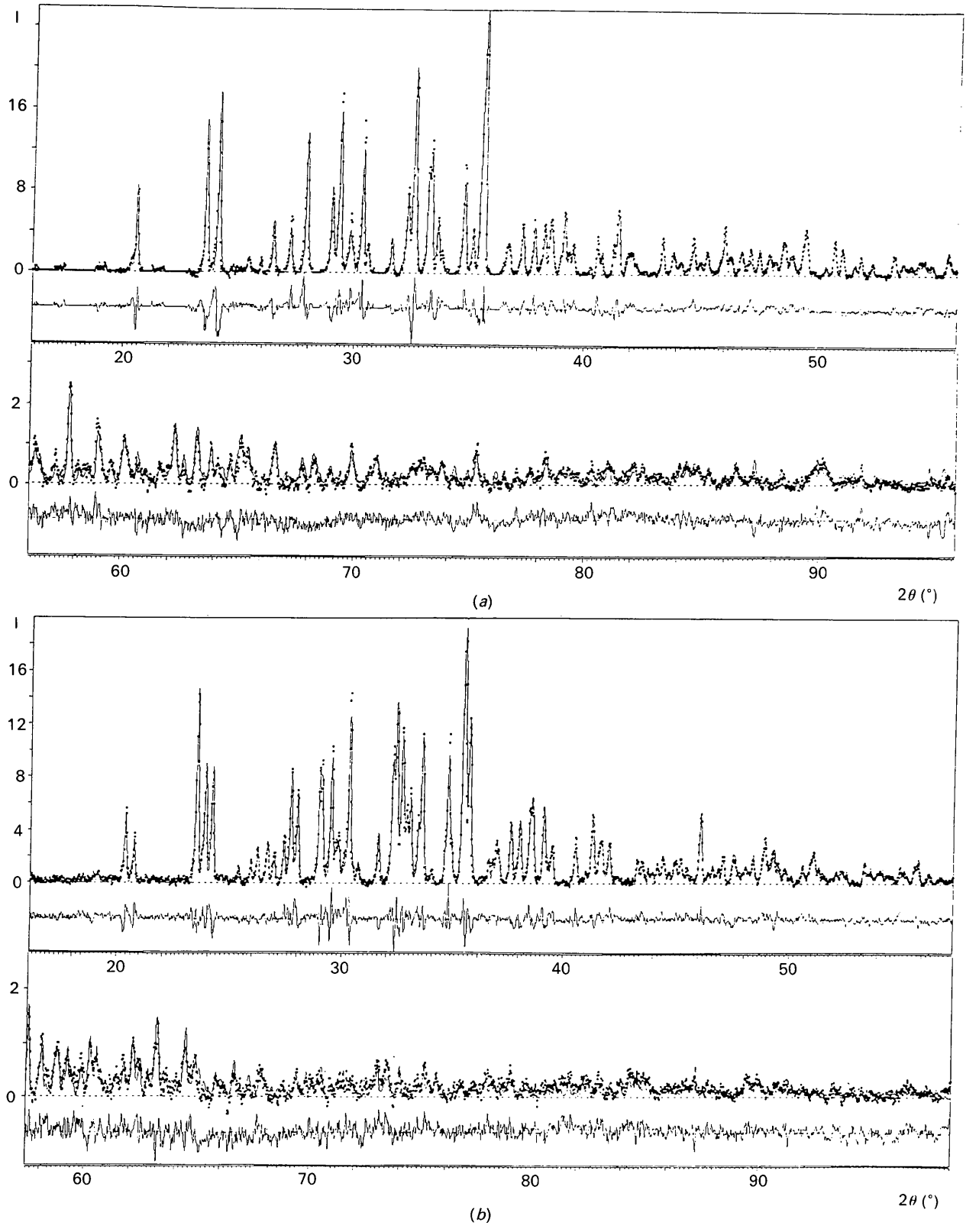

Fig. 1. Measured and calculated X-ray patterns together with their difference profiles at (*a*) 120 and (*b*) 100 K; the intensity is given in an arbitrary scale.

differences in the angles O(1)—C(1)—O(2), O(2)—C(1)—C(2), O(3)—C(2)—C(1), O(3)—C(2)—C(3) and O(6)—C(4)—C(3), as well as in the Na—O(1), Na—O(3) and Na—O(5) distances, were observed. Apparently, the differences in the bond angles were not accompanied by any significant change in the torsion angles; the same conformation of the tartaric anion was thus found. The powder method, although less precise, proved almost as useful as a typical single-crystal measurement; a reliable comparison of the paraelectric structure at 120 K and the polar structure at 100 K can be performed.

Since the expected superstructure features in the polar phase were not detected by the Guinier photographic method, the structure was refined using unit-cell parameters similar to those of the non-polar phase, without *a*-axis doubling.

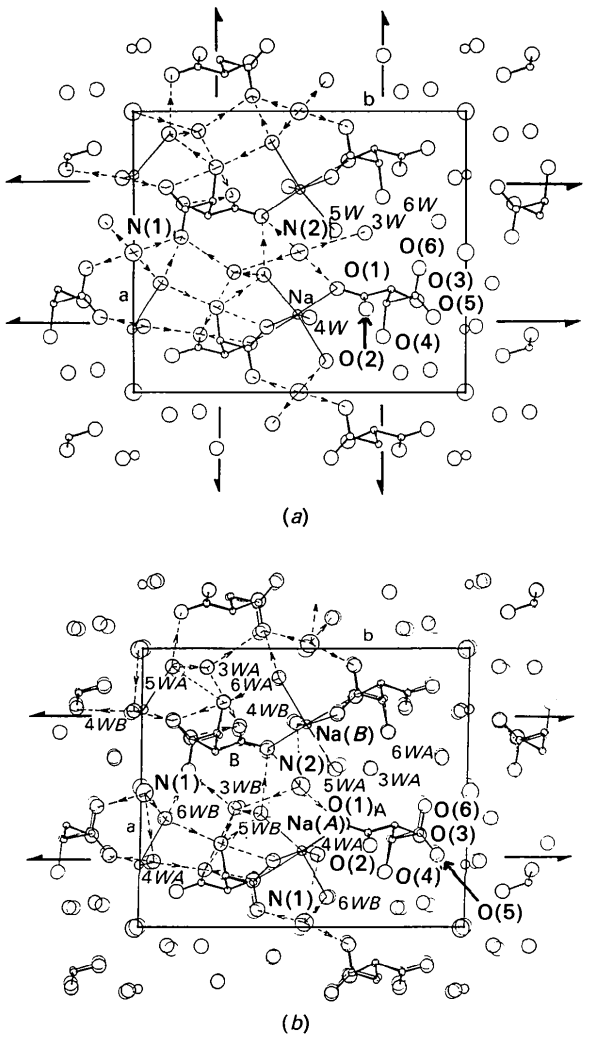

Fig. 2. The scheme of cation environments (full lines) and hydrogen bonding (broken lines with arrows pointing towards a hydrogen acceptor) shown in the **ab** projection of the NAT crystal structure: (*a*) in the paraelectric phase at 120 K and (*b*) in the ferroelectric phase at 100 K (thicker lines) superimposed on the paraelectric structure.

Table 2. *Fractional atomic coordinates and isotropic thermal parameters* U_{iso} (Å^2) *with e.s.d.'s in parentheses*

	x	*y*	*z*	U_{iso}
120 K ($P2_12_12$)				
Na	0.7242 (8)	0.4969 (5)	0.5041 (18)	0.028 (9)
O(1)	0.629 (1)	0.615 (1)	0.345 (2)	0.036 (20)
O(2)	0.704 (1)	0.700 (1)	0.094 (2)	0.026 (20)
O(3)	0.674 (1)	0.853 (1)	0.310 (2)	0.004 (10)
O(4)	0.802 (4)	0.751 (1)	0.636 (2)	0.030 (20)
O(5)	0.733 (1)	0.903 (1)	0.828 (2)	0.014 (10)
O(6)	0.556 (1)	0.869 (1)	0.858 (2)	0.026 (20)
C(1)	0.658 (2)	0.694 (1)	0.276 (3)	0.046 (30)
C(2)	0.633 (2)	0.775 (1)	0.426 (3)	0.033 (30)
C(3)	0.683 (1)	0.762 (1)	0.650 (3)	0.088 (40)
C(4)	0.655 (4)	0.847 (2)	0.791 (4)	0.047 (30)
N(1)	1/2	0	0.151 (4)	0.062 (40)
N(2)	1/2	1/2	0.060 (3)	0.026 (30)
O(3*W*)	0.430 (1)	0.696 (1)	0.975 (2)	0.022 (20)
O(4*W*)	0.735 (1)	0.532 (1)	0.885 (2)	0.021 (20)
O(5*W*)	0.421 (1)	0.606 (2)	0.566 (2)	0.027 (20)
O(6*W*)	0.390 (1)	0.918 (1)	0.537 (2)	0.004 (10)
100 K ($P12_11$, origin at $\frac{1}{4}00$)				
Na(*A*)	0.725 (2)	0.496 (2)	0.502 (3)	0.023 (4)
O(1*A*)	0.630 (2)	0.616 (2)	0.342 (5)	0.028 (7)
O(2*A*)	0.707 (2)	0.701 (2)	0.096 (4)	0.039 (7)
O(3*A*)	0.670 (3)	0.854 (2)	0.304 (5)	0.038 (6)
O(4*A*)	0.800 (2)	0.747 (2)	0.666 (4)	0.036 (7)
O(5*A*)	0.740 (2)	0.909 (2)	0.829 (5)	0.040 (8)
O(6*A*)	0.565 (2)	0.869 (2)	0.838 (5)	0.065 (9)
C(1*A*)	0.663 (4)	0.694 (1)	0.277 (5)	0.064 (10)
C(2*A*)	0.636 (3)	0.775 (1)	0.425 (5)	0.030 (10)
C(3*A*)	0.685 (2)	0.768 (2)	0.651 (4)	0.054 (10)
C(4*A*)	0.664 (2)	0.854 (2)	0.786 (8)	0.078 (10)
O(3*WA*)	0.432 (2)	0.699 (2)	0.953 (5)	0.049 (8)
O(4*WA*)	0.738 (2)	0.542 (2)	0.875 (5)	0.017 (6)
O(5*WA*)	0.434 (3)	0.591 (2)	0.585 (5)	0.059 (8)
O(6*WA*)	0.396 (3)	0.920 (2)	0.524 (5)	0.017 (6)
N(1)	0.517 (3)	0.010 (3)	0.129 (5)	0.066 (10)
N(2)	0.495 (4)	0.490 (3)	0.060 (6)	0.034 (8)
Na(*B*)	0.277 (2)	0.505 (1)	0.516 (3)	0.050 (5)
O(1*B*)	0.360 (2)	0.387 (1)	0.359 (4)	0.045 (8)
O(2*B*)	0.282 (2)	0.302 (2)	0.106 (4)	0.077 (9)
O(3*B*)	0.324 (2)	0.150 (1)	0.312 (4)	0.022 (6)
O(4*B*)	0.194 (2)	0.251 (2)	0.615 (4)	0.034 (7)
O(5*B*)	0.261 (2)	0.095 (1)	0.806 (6)	0.030 (7)
O(6*B*)	0.438 (2)	0.145 (1)	0.847 (6)	0.046 (7)
C(1*B*)	0.336 (4)	0.308 (1)	0.280 (5)	0.054 (10)
C(2*B*)	0.373 (2)	0.227 (1)	0.421 (3)	0.022 (9)
C(3*B*)	0.309 (2)	0.231 (1)	0.630 (3)	0.071 (10)
C(4*B*)	0.335 (2)	0.157 (1)	0.801 (8)	0.025 (9)
O(3*WB*)	0.572 (2)	0.290 (2)	0.952 (5)	0.028 (7)
O(4*WB*)	0.272 (2)	0.475 (2)	0.887 (5)	0.068 (9)
O(5*WB*)	0.590 (2)	0.370 (2)	0.551 (5)	0.065 (8)
O(6*WB*)	0.610 (3)	0.074 (2)	0.553 (6)	0.019 (6)

In the ferroelectric phase there are two symmetry independent tartrate anions *A* and *B*. The geometry of *A* remains similar to that of the paraelectric phase, whereas *B* reveals significant differences in bond angles and torsion angles. The most striking of these seem to follow the changes of the hydroxyl O(4) group function in the crystal structure. The hydroxyl O(4*A*) group accepts hydrogen bonds from the water

Table 3. *Important geometric parameters of (a) the tartaric anions, (b) the environment of cations and (c) water molecules*

Bond lengths and distances (shorter than 3.20 Å) are given in Å, bond angles and torsional angles in ° with e.s.d.'s in parentheses. Data from single-crystal refinement (Brożek & Stadnicka, 1994) are marked by asterisks.

	120 K* (On cooling)	120 K (On heating)		100 K (On heating)		
(*a*) Tartaric anion			*A*		*B*	
O(1)—C(1)	1.268 (3)	1.27 (2)		1.26 (4)		1.26 (3)
O(2)—C(1)	1.251 (3)	1.26 (2)		1.26 (5)		1.26 (4)
O(3)—C(2)	1.426 (3)	1.42 (2)		1.42 (4)		1.42 (3)
O(4)—C(3)	1.423 (3)	1.44 (5)		1.43 (4)		1.42 (4)
O(5)—C(4)	1.246 (3)	1.26 (2)		1.25 (4)		1.27 (3)
O(6)—C(4)	1.262 (3)	1.28 (2)		1.26 (4)		1.29 (4)
C(1)—C(2)	1.522 (3)	1.52 (3)		1.53 (4)		1.53 (3)
C(2)—C(3)	1.519 (3)	1.53 (3)		1.52 (4)		1.52 (3)
C(3)—C(4)	1.520 (3)	1.54 (3)		1.52 (4)		1.53 (4)
O(3)···O(2)	2.606 (2)	2.59 (2)	O(3*A*)···O(2*A*)	2.59 (3)	O(3*B*)···O(2*B*)	2.58 (3)
O(3)···O(5^{i})		[3.15 (2)]	O(3*A*)···O(5*A*^{i})	[3.18 (4)]		
O(3)···O(6^{i})		[3.14 (2)]	O(3*A*)···O(6*A*^{i})	[3.14 (4)]		
O(4)···O(5)	2.666 (2)	2.62 (2)	O(4*A*)···O(5*A*)	2.65 (4)	O(4*B*)···O(5*B*)	2.66 (3)
O(4)···O(2^{ii})	[3.190 (3)]	[3.15 (2)]	O(4*A*)···O(2*A*^{ii})	2.99 (4)		
O(4)···O(3*W*^{iii})	[3.123 (3)]	2.97 (3)	O(4*A*)···O(3*WB*^{v})	2.88 (4)	O(4*B*)···O(3*WA*^{v})	[3.20 (4)]
O(4)···O(5*W*^{vi})	2.828 (3)	2.80 (3)	O(4*A*)···O(5*WB*^{vii})	2.61 (4)	O(4*B*)···O(5*WA*^{viii})	[3.04 (4)]
O(4)···O(6*W*^{vi})	2.773 (2)	2.86 (3)	O(4*A*)···O(6*WB*^{vii})	[3.05 (4)]	O(4*B*)···O(6*WA*^{viii})	2.79 (4)

Symmetry codes: (i) $x, y, z-1$; (ii) $x, y, z+1$; (iii) $x+\frac{1}{2}, -y+\frac{3}{2}, -z+2$; (iv) $-x+\frac{3}{2}, y+\frac{1}{2}, -z+2$; (v) $-x+\frac{1}{2}, y-\frac{1}{2}, -z+2$; (vi) $x+\frac{1}{2}, -y+\frac{3}{2}, -z+1$; (vii) $-x+\frac{3}{2}, y+\frac{1}{2}, -z+1$; (viii) $-x+\frac{3}{2}, y-\frac{1}{2}, -z+1$.

O(1)—C(1)—O(2)	126.2 (2)	119 (2)		120 (2)		121 (2)
O(1)—C(1)—C(2)	117.1 (2)	115 (2)		115 (3)		114 (2)
O(2)—C(1)—C(2)	116.8 (2)	126 (2)		125 (2)		125 (2)
O(3)—C(2)—C(1)	111.1 (2)	103 (1)		103 (2)		102 (2)
O(3)—C(2)—C(3)	108.5 (2)	115 (1)		115 (2)		103 (2)
O(4)—C(3)—C(2)	110.3 (2)	111 (1)		116 (2)		118 (2)
O(4)—C(3)—C(4)	112.4 (2)	110 (1)		108 (2)		112 (2)
C(1)—C(2)—C(3)	111.4 (2)	112 (1)		115 (2)		108 (2)
C(2)—C(3)—C(4)	110.0 (2)	109 (1)		113 (2)		118 (2)
O(5)—C(4)—O(6)	125.6 (2)	123 (2)		123 (3)		126 (2)
O(5)—C(4)—C(3)	117.5 (2)	117 (1)		120 (3)		112 (2)
O(6)—C(4)—C(3)	116.9 (2)	120 (1)		117 (3)		116 (2)
O(1)—C(1)—C(2)—O(3)	179.3 (2)	180 (2)		−174 (3)		173 (3)
O(2)—C(1)—C(2)—O(3)	1.6 (3)	0 (2)		1 (4)		−4 (4)
O(1)—C(1)—C(2)—C(3)	59.6 (3)	56 (2)		60 (4)		65 (3)
O(2)—C(1)—C(2)—C(3)	−119.5 (2)	−124 (2)		−125 (4)		−112 (3)
H(O3)—O(3)—C(2)—C(1)	−18.9 (7)					
C(1)—C(2)—C(3)—O(4)	56.3 (3)	58 (2)		50 (3)		43 (3)
O(3)—C(2)—C(3)—O(4)	−66.2 (2)	−58 (2)		−69 (3)		−65 (3)
C(1)—C(2)—C(3)—C(4)	−179.1 (2)	180 (2)		175 (3)		−178 (2)
O(3)—C(2)—C(3)—C(4)	58.4 (2)	63 (2)		56 (3)		74 (3)
O(6)—C(4)—C(3)—O(4)	−165.4 (2)	−167 (2)		−162 (3)		−170 (3)
O(5)—C(4)—C(3)—O(4)	15.7 (3)	15 (3)		23 (4)		37 (3)
O(6)—C(4)—C(3)—C(2)	71.2 (3)	71 (2)		68 (4)		49 (4)
O(5)—C(4)—C(3)—C(2)	−107.7 (3)	−106 (2)		−107 (3)		−104 (3)
H(O4)—O(4)—C(3)—C(4)	−56.3 (8)					
Dihedral angle between planes O(1)O(2)C(1)C(2)O(3) and O(4)C(3)C(4)O(5)O(6):	50.80 (7)	54 (1)		60 (1)		55 (1)
(*b*) Na^+ cation						
Na—O(1)	2.375 (2)	2.27 (2)	Na(*A*)—O(1*A*)	2.29 (3)	Na(*B*)—O(1*B*)	2.22 (3)
Na—O(4*W*)	2.350 (2)	2.41 (2)	Na(*A*)—O(4*WA*)	2.41 (3)	Na(*B*)—O(4*WB*)	2.34 (4)
Na—O(3^{i})	2.484 (2)	2.66 (2)	Na(*A*)—O(3*A*^{i})	2.69 (3)	Na(*B*)—O(3*B*^{ii})	2.66 (3)
Na—O(5^{i})	2.449 (2)	2.51 (2)	Na(*A*)—O(5*A*^{i})	2.45 (3)	Na(*B*)—O(5*B*^{ii})	2.42 (4)
Na—O(5*W*^{iii})	2.349 (2)	2.32 (2)	Na(*A*)—O(5*WB*^{v})	2.47 (3)	Na(*B*)—O(5*WA*^{iv})	2.31 (4)
Na—O(6*W*^{v})	2.349 (2)	2.35 (1)	Na(*A*)—O(6*WB*^{vi})	2.33 (4)	Na(*B*)—O(6*WA*^{vii})	2.44 (4)

Symmetry codes: (i) $-x+\frac{3}{2}, y-\frac{1}{2}, -z+1$; (ii) $-x+\frac{1}{2}, y+\frac{1}{2}, -z+1$; (iii) $-x+1, -y+1, z$; (iv) x, y, z; (v) $x+\frac{1}{2}, -y+\frac{3}{2}, -z+1$; (vi) $-x+\frac{3}{2}, y+\frac{1}{2}, -z+1$; (vii) $-x+\frac{1}{2}, y-\frac{1}{2}, -z+1$.

Ammonium cations						
N(1)···O(6^{i})	2.835 (2)	2.79 (2)	N(1)···O(6*A*^{i})	2.79 (5)		
N(1)···O(6*W*^{vi})	2.947 (3)	2.97 (3)	N(1)···O(6*WA*^{vi})	[3.16 (5)]		
N(1)···O(6^{ii})	2.835 (2)	2.79 (2)	N(1)···O(6*B*^{iii})	2.77 (5)		

Table 3 (*cont.*)

	120 K* (On cooling)	120 K (On heating)		100 K (On heating)		
			A		*B*	
N(1)···O(6*W*^{ii})	2.947 (3)	2.97 (3)	N(1)···O(6*WB*)	2.98 (5)		
N(1)···O(4*W*^{iv})			N(1)···O(4*WA*^{v})	3.00 (5)		
N(1)···O(3^{vi})	[3.152 (2)]	[3.14 (2)]	N(1)···O(3*A*^{vi})	[3.10 (5)]		
N(2)···O(1)	2.876 (3)	2.87 (2)	N(2)···O(1*A*)	2.99 (5)		
N(2)···O(3*W*^{iii})	2.995 (2)	2.98 (1)	N(2)···O(3*WA*^{iii})	[3.18 (5)]		
N(2)···O(1^{ii})	2.876 (3)	2.87 (2)	N(2)···O(1*B*)	2.91 (5)		
N(2)···O(3*W*^{ii})	2.995 (2)	2.98 (1)	N(2)···O(3*WB*^{iii})	3.10 (5)		
N(2)···O(4*W*^{vi})	[3.091 (2)]	[3.07 (2)]	N(2)···O(4*WB*^{iii})	2.90 (5)		

Symmetry codes: (i) $x, y-1, z-1$; (ii) $-x+1, -y+1, z$; (iii) $x, y, z-1$; (iv) $x-\frac{1}{2}, -y+\frac{1}{2}, -z+1$; (v) $-x+\frac{3}{2}, y-\frac{1}{2}, -z+1$; (vi) $x, y-1, z$.

(*c*) Water molecules

O(3*W*)···O(5*W*)	2.771 (3)	2.84 (2)	O(3*WA*)···O(5*WA*)	2.76 (4)	O(3*WB*)···O(5*WB*)	2.75 (4)
O(3*W*)···O(6)	2.773 (2)	2.89 (2)	O(3*WA*)···O(6*A*)	3.02 (4)	O(3*WB*)···O(6*B*)	2.72 (4)
O(3*W*)···N(2^{i})	2.995 (2)	2.98 (1)	O(3*WA*)···N(2^{i})	[3.18 (5)]	O(3*WB*)···N(2^{i})	3.10 (5)
O(3*W*)···O(2^{iii})	3.100 (3)	[3.14 (2)]	O(3*WA*)···O(2*B*^{iii})	3.02 (4)	O(3*WB*)···O(2*A*^{iv})	2.99 (4)
O(3*W*)···O(4^{v})	[3.123 (3)]	2.97 (3)	O(3*WA*)···O(4*B*^{vi})	[3.20 (4)]	O(3*WB*)···O(4*A*^{vii})	2.88 (4)
O(3*W*)···O(5^{v})	[3.209 (3)]	[3.03 (2)]	O(3*WA*)···O(5*B*^{vi})	[3.18 (4)]	O(3*WB*)···O(5*A*^{viii})	[3.14 (5)]
O(4*W*)···Na	2.350 (2)	2.41 (2)	O(4*WA*)···Na(*A*)	2.41 (3)	O(4*WB*)···Na(*B*)	2.34 (4)
O(4*W*)···O(5^{vii})	2.734 (3)	2.60 (2)	O(4*WA*)···O(5*A*^{vii})	2.66 (4)	O(4*WB*)···O(5*B*^{viii})	2.60 (4)
O(4*W*)···O(2^{i})	2.765 (2)	2.76 (2)	O(4*WA*)···O(2*A*^{i})	2.70 (3)	O(4*WB*)···O(2*B*)	2.84 (4)
O(4*W*)···O(3)	[3.096 (3)]	[3.05 (2)]	O(4*WA*)···O(3*A*)	[3.15 (4)]	O(4*WB*)···O(3*B*)	[3.03 (4)]
O(4*W*)···N(2^{i})	[3.091 (2)]	[3.07 (2)]			O(4*WB*)···N(2^{i})	2.90 (5)
O(4*W*)···N(1^{ix})			O(4*WA*)···N(1^{ix})	3.00 (5)		
O(5*W*)···Na^{x}	2.349 (2)	2.32 (2)	O(5*WA*)···Na(*B*^{xi})	2.31 (4)	O(5*WB*)···Na(*A*^{xi})	2.47 (3)
O(5*W*)···O(1)	2.736 (3)	2.87 (2)	O(5*WA*)···O(1*A*)	2.85 (4)	O(5*WB*)···O(1*B*)	[3.02 (4)]
O(5*W*)···O(3*W*)	2.771 (3)	2.84 (2)	O(5*WA*)···O(3*WA*)	2.76 (4)	O(5*WB*)···O(3*WB*)	2.75 (4)
O(5*W*)···O(4^{ii})	2.828 (2)	2.80 (3)	O(5*WA*)···O(4*B*^{iii})	[3.04 (4)]	O(5*WB*)···O(4*A*^{iv})	2.61 (4)
O(6*W*)···Na^{ii}	2.349 (2)	2.35 (1)	O(6*WA*)···Na(*B*^{iii})	2.44 (4)	O(6*WB*)···Na(*A*^{iv})	2.33 (4)
O(6*W*)···O(4^{ii})	2.773 (2)	2.86 (3)	O(6*WA*)···O(4*B*^{iii})	2.79 (4)	O(6*WB*)···O(4*A*^{iv})	3.05 (4)
O(6*W*)···O(6)	2.897 (2)	2.95 (2)	O(6*WA*)···O(6*A*)	2.90 (4)	O(6*WB*)···O(6*B*)	2.97 (5)
O(6*W*)···N(1^{xii})	2.947 (3)	2.97 (3)	O(6*WA*)···N(1^{xiii})	[3.16 (5)]	O(6*WB*)···N(1^{xi})	2.98 (5)

Symmetry codes: (i) $x, y, z+1$; (ii) $x-\frac{1}{2}, -y+\frac{3}{2}, -z+1$; (iii) $-x+\frac{1}{2}, y+\frac{1}{2}, -z+1$; (iv) $-x+\frac{3}{2}, y-\frac{1}{2}, -z+1$; (v) $x-\frac{1}{2}, -y+\frac{3}{2}, -z+2$; (vi) $-x+\frac{1}{2}, y-\frac{1}{2}, -z+2$; (vii) $-x+\frac{3}{2}, y-\frac{1}{2}, -z+2$; (viii) $-x+\frac{1}{2}, y+\frac{1}{2}, -z+2$; (ix) $-x+\frac{3}{2}, y+\frac{1}{2}, -z+1$; (x) $-x+1, -y+1, z$; (xi) x, y, z; (xii) $-x+1, y+1, z$; (xiii) $x, y+1, z$.

molecules O(3*WB*) and O(6*WB*), similar to the situation in the paraelectric phase, and remains a hydrogen donor for the O(5*WB*) water molecule. On the contrary, the hydroxyl O(4*B*) participates in an intramolecular hydrogen bond with the carboxylic O(5*B*) and accepts a hydrogen bond from the water molecule O(6*WA*).

The environments of both $Na(A)^+$ and $Na(B)^+$ cations consist of the same set of O atoms, but differ in the appropriate distances and angles. The distances $Na(A)^+\cdots O(5WB)$ and $Na(B)^+\cdots O(6WA)$ are markedly longer than those in the paraelectric phase.

Both ammonium N atoms, N(1) and N(2), lose their twofold symmetry in the ferroelectric phase transition, shift significantly and change their orientation in relation to the O atoms of the carboxyl groups and water molecules. The hydrogen bond N(1)···O(6*WA*) breaks and N(1)···O(4*WB*) forms instead. Similarly, the N(2) ammonium cation moves away from the water molecule O(3*WA*) to form a new hydrogen bond with the O(4*WB*) molecule. Such a reorientation of the ammonium cations with respect to the paraelectric phase is accompanied by a relative displacement of water molecules, decreasing in the order O(5*W*) > O(4*W*) > O(3*W*) > O(6*W*) (Table 4), and a rearrangement of their hydrogen bonds, since all are involved in the hydrogen-bonding network.

The water O(3*W*) forms four hydrogen bonds in the paraelectric phase. It becomes two symmetry-independent water molecules O(3*WA*) and O(3*WB*) in the ferroelectric phase. Whereas O(3*WA*) has only three O atoms in its environment (up to 3.20 Å), O(3*WB*) forms, together with its five neighbours, a distorted trigonal bipyramid [involving N(2) as a donor and O(4*A*) as an acceptor of H atoms]. The water molecule O(4*WA*) has three neighbours in the paraelectric phase and four in the ferroelectric phase accepting an additional H atom from the N(1) cation. O(4*WB*) behaves similarly with respect to the N(2) cation. O(5*WA*) and O(5*WB*) lose the hydroxyl O(4*B*) and the carboxyl O(1*B*), respectively, leaving both with only three neighbours. O(6*WA*) detaches from N(1) and O(6*WB*) preserves its environment from the paraelectric phase, although its distance to O(4*A*) increases.

In general, the relationship between the paraelectric and ferroelectric phases may be described in

Table 4. *Values of state shifts* (Å) *in NAT crystals at* 100 K

$|\Delta| = [\Delta^2(x)a^2 + \Delta^2(y)b^2 + \Delta^2(z)c^2 + 2\Delta(x)\Delta(z)ac\cos\beta]^{0.5}$ and $|\Delta y| = [\Delta^2(y)b^2]^{0.5}$ with standard deviations estimated from coordinate and unit-cell parameter e.s.d.'s in parentheses. The fractional coordinates are expressed against the monoclinic unit-cell parameters at 100 K.

	Δx	Δy	Δz	$\lvert\Delta y\rvert$	$\lvert\Delta\rvert$
Na(*A*)/Na(*B*)	0.00651	−0.00130	−0.01457	0.02 (2)	0.12 (3)
O(1*A*)/O(1*B*)	0.01614	−0.00272	−0.01648	0.04 (3)	0.22 (4)
O(2*A*)/O(2*B*)	0.01221	−0.00320	−0.00994	0.05 (3)	0.17 (4)
O(3*A*)/O(3*B*)	0.01126	−0.00392	−0.00759	0.06 (3)	0.16 (4)
O(4*A*)/O(4*B*)	0.01775	0.00141	0.05121	0.02 (3)	0.38 (4)
O(5*A*)/O(5*B*)	0.01375	−0.00428	0.02294	0.06 (3)	0.23 (4)
O(6*A*)/O(6*B*)	0.01166	−0.01327	−0.00911	0.19 (3)	0.24 (4)
C(1*A*)/C(1*B*)	0.00598	−0.00227	−0.00321	0.03 (3)	0.08 (6)
C(2*A*)/C(2*B*)	−0.00105	−0.00204	0.00391	0.03 (3)	0.04 (3)
C(3*A*)/C(3*B*)	0.01752	0.00139	0.02142	0.02 (3)	0.25 (4)
C(4*A*)/C(4*B*)	0.01552	−0.01080	−0.01443	0.16 (3)	0.26 (4)
N(1)/N(1′)	−0.03257	−0.02072	0.00000	0.30 (6)	0.50 (6)
N(2)/N(2′)	0.01046	0.02036	0.00000	0.29 (6)	0.32 (6)
O(3*WA*)/O(3*WB*)	0.01312	0.01049	0.00098	0.15 (4)	0.22 (4)
O(4*WA*)/O(4*WB*)	0.00541	−0.01752	−0.01214	0.25 (4)	0.27 (4)
O(5*WA*)/O(5*WB*)	−0.01362	0.03838	0.03337	0.55 (4)	0.61 (4)
O(6*WA*)/O(6*WB*)	0.00397	0.00598	−0.02918	0.09 (4)	0.21 (5)

terms of the relative displacements (also called *state shifts*) for all atoms in the unit cell. In the case of NAT, the ferroelectric phase transition occurs at 109 K, with the loss of the twofold symmetry along [001], on cooling. Thus, the symmetry changes from $P2_12_12$ to $P12_11$ and so the low-temperature phase becomes polar ($\mathbf{P}_s \| [010]$). The two possible ferroelectric orientation states are related by a pseudo-2[001] operation. This symmetry can be used to calculate the relative atomic displacements caused by a hypothetical ferroelectric switching, such that the rotation operation (R) is applied to the atomic coordinates x_i in one particular orientation; the resulting position is compared with the pseudo-symmetrically related atomic position x_j in the same orientation state. Differences between these positions are defined as $\Delta_i = Rx_i - x_j$ (see Fig. 3) and, expressed in Å, give the state shifts for various atoms. Table 4 presents Δ_i for each atom defined by its components with respect to the monoclinic unit-cell parameters at 100 K

$$\begin{pmatrix}\Delta x\\ \Delta y\\ \Delta z\end{pmatrix} = \begin{pmatrix}x_i'\\ y_i'\\ z_i'\end{pmatrix} - \begin{pmatrix}x_j\\ y_j\\ z_j\end{pmatrix}$$

$$= \begin{pmatrix}\bar{1} & 0 & \sin(\beta-90°)\\ 0 & \bar{1} & 0\\ 0 & 0 & 1\end{pmatrix}\begin{pmatrix}x_i\\ y_i\\ z_i\end{pmatrix} - \begin{pmatrix}x_j\\ y_j\\ z_j\end{pmatrix},$$

as well as by its absolute value $|\Delta_i|$ in Å. The largest relative displacements of atoms ($|\Delta| > 0.30$ Å) in the ferroelectric phase with respect to the paraelectric structure were observed for O(5*W*) > N(1) > (O)4 > N(2) in decreasing sequence. These were accompanied by a cooperative process involving atomic reorientation and hydrogen-bond reorganization, as described above. The complex structural mechanism of the phase transition would seem to explain the peculiar behaviour of NAT crystals in the ferroelectric phase when compared with RS, *e.g.* its spontaneous polarization cannot be reversed by an electric field but by a shearing stress of *ca* 98 kg cm^{-2}, producing a mono-domain sample (Takagi & Makita, 1958). Knowing structural changes at the phase transition, we can estimate $\mathbf{P}_s$ from a simple point-charge model using the formula $\mathbf{P}_s = 1/V\sum_{i=1}^{N/2} Z_i\Delta_i$ (Lines & Glass, 1977), where V is the unit-cell volume, Z_i are the effective charges and Δ_i the atomic displacement vectors which give a measure of the change in atomic position on switching. Here only obviously charged atoms were considered: the carboxylic O atoms with $Z = -0.5$ e and all the cations with $Z = +1.0$ e. Relative displacements of these atoms along the b axis (y-components of the state shifts, $|\Delta_y|$) were taken with the appropriate signs from column Δy (Table 4). The resultant dipole moments for the water molecules in the unit cell, although certainly non-zero in the ferroelectric phase, were neglected. The $\mathbf{P}_s$ value of $+0.22\,(1) \times 10^{-6}$ C cm^{-2},* obtained for NAT crystals at 100 K, was in impressive agreement with that found experimentally, $|\mathbf{P}_s| = 0.21 \times 10^{-6}$ C cm^{-2} at 92 K (Takagi & Makita, 1958). It is worthwhile mentioning that for deuterated NAT,

* Within the expression for $\mathbf{P}_s$ variance: $\sigma^2(\mathbf{P}_s) = (\delta\mathbf{P}_s/\delta V)^2\sigma^2(V) + (\delta\mathbf{P}_s/\delta b)^2\sigma^2(b) + (\delta\mathbf{P}_s/\delta V)(\delta\mathbf{P}_s/\delta b)\sigma(V)\sigma(b) + (\delta\mathbf{P}_s/\delta e)^2\sigma^2(e) + \sum_{i=1}^{N/2}[\delta\mathbf{P}_s/\delta(\Delta_i y)]^2\sigma^2(\Delta_i y)$, the last part was limiting $[0.72 \times 10^{-16}$ (C cm^{-2})$^2]$, since the others were of the order 10^{-23}. Thus, the standard deviation of $\mathbf{P}_s$ was found to be 0.85×10^{-8} C cm^{-2}.

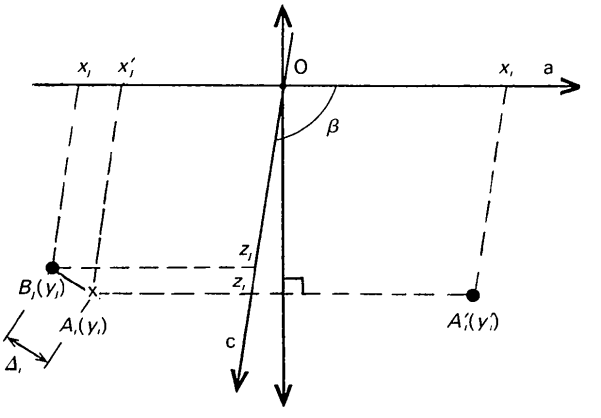

Fig. 3. Illustration of getting Δ_i shift states in projection onto **ac**. Notice that the origin of the orthorhombic unit cell is preserved in the monoclinic phase. Atom $A_i(x_i,y_i,z_i)$ is rotated by a pseudo-twofold axis perpendicular to **ab** to the position $A_i'(x_i',y_i',z_i')$, which should be compared with coordinates of the closest atom of the same type [here $B_j(x_j,y_j,z_j)$].

$NaND_4C_4H_2D_2O_6.4D_2O$, the spontaneous polarization calculated only from the distortion of ND_4^+ cations, determined by NMR, yielded 52% of the experimental value quoted above (El Saffar & Peterson, 1976).

We are grateful to Professor A. Simon's group, MPI für Festkörperforschung, Stuttgart, for making the Guinier photographs and to Professor H. Burzlaff, Erlangen-Nürnberg University, for inspiration and helpful discussion.

References

Aizu, K. (1971). *J. Phys. Soc. Jpn*, **31**, 1521–1526.
Aizu, K. (1984). *J. Phys. Soc. Jpn*, **53**, 1775–1782.
Aizu, K. (1986*a*). *J. Phys. Soc. Jpn*, **55**, 1663–1670.
Aizu, K. (1986*b*). *J. Phys. Soc. Jpn*, **55**, 4302–4308.
Aizu, K. (1990). *J. Phys. Soc. Jpn*, **59**, 1293–1298.
Beevers, C. A. & Hughes, W. (1941). *Proc. R. Soc. London Ser. A*, **177**, 251–259.
Brożek, Z. & Stadnicka, K. (1994). *Acta Cryst.* B**50**, 59–68.
El Saffar, Z. M. & Peterson, E. M. (1976). *J. Chem. Phys.* **64**, 3283–3290.
Iizumi, M. & Gesi, K. (1978). *J. Phys. Soc. Jpn*, **45**, 711–712.
Ishibashi, Y. & Takagi, Y. (1975). *J. Phys. Soc. Jpn*, **38**, 1715–1719.
Johnson, C. K. (1971). *ORTEP*II. Report ORNL-3794, revised. Oak Ridge National Laboratory, Tennessee, USA.
Jona, F. & Shirane, G. (1962). *Ferroelectric Crystals*. Oxford: Pergamon Press.
Kuroda, R. & Mason, F. (1981). *J. Chem. Soc. Dalton Trans.* pp. 1268–1273.
Lines, M. E. & Glass, A. M. (1977). *Principle and Applications of Ferroelectrics and Related Materials*. Oxford: Clarendon Press.
Lowry, T. M. (1964). *Optical Rotatory Power*. New York: Dover Publications.
Mucha, D. & Łasocha, W. (1994). *J. Appl. Cryst.* **27**, 201–202.
Nardelli, M. (1983). *Comput. Chem.* **7**, 95–98.
Sannikov, D. Z. & Levanyuk, A. P. (1977). *Solid State Phys.* **19**, 118–120.
Sawada, A. & Takagi, Y. (1971). *J. Phys. Soc. Jpn*, **31**, 952.
Sawada, A. & Takagi, Y. (1972). *J. Phys. Soc. Jpn*, **33**, 1071–1075.
Shkuratova, I. G., Kiosse, G. A. & Malinovskii, T. I. (1979). *Izv. Akad. Nauk SSSR, Ser. Fiz.* **43**, 1685–1690.
Takagi, Y. & Makita, Y. (1958). *J. Phys. Soc. Jpn*, **13**, 272–277.

Acta Cryst. (1994). B**50**, 472–479

Structure of the Stable Phase of Methylhydrazine – First Observations of Phase Transitions

By M. Foulon, N. Lebrun, M. Muller and A. Amazzal

Laboratoire de Dynamique et Structure des Matériaux URA CNRS 801, *UFR de Physique, Université des Sciences et Technologies de Lille*, 59655 *Villeneuve d'Ascq CEDEX, France*

and M. T. Cohen-Adad

Laboratoire de Physicochimie des Matériaux Luminescents, UA CNRS 442, *Université Claude Bernard Lyon* I, 43 *boulevard du* 11 *Novembre* 1918, 69622 *Villeurbanne CEDEX, France*

(*Received* 16 *July* 1993; *accepted* 21 *March* 1994)

Abstract

A study of methylhydrazine, CH_3NHNH_2, has provided the following data: monoclinic system, $P2_1/c$, $a = 10.043$ (10), $b = 3.925$ (5), $c = 7.670$ (8) Å, $\beta = 107.28$ (10)°, $V = 288.7$ (1.1) Å^3, $Z = 4$, $M_r = 46.07$, $D_x = 1.06$ g cm^{-3}, λ(Mo $K\alpha$) = 0.7107 Å, $\mu = 0.81$ cm^{-1}, $F(000) = 104$, $T = 179$ K, $R = 0.039$ for 703 reflexions [$I \geq 3\sigma(I)$]. A single crystal was grown *in situ* from the liquid by an adapted Bridgman method. The crystallographic cell contains equimolar proportions of isomers with the outer conformation. The internal rotation angle for the NH_2 group around the N—C bond is 82°. The molecular volume is estimated to be 48.9 Å^3, which leads to a relatively high compactness factor (0.68). The N—C molecular bonds are parallel to the crystallographic *a* axis. The structure may be described by planes of molecules, linked by van der Waals contacts, parallel to the **b**, **c** plane and related by **a**/2 translations. In each plane, one molecule is linked to four neighbours by weak hydrogen bonds. Phase transformations, as observed by DSC (differential scanning calorimetry) and Raman spectroscopy, are detailed. One glassy phase is obtained by quenching the liquid. One metastable phase appears by rapid cooling. This metastable